ARL-TR-9508 ● AUG 2022

DEVCOM ARMY RESEARCH LABORATORY

Characterization of Fe_3O_4 Magnetosomes by Small-angle X-ray Scattering

by Frederick L Beyer, Mark A Allen, and Justin P Jahnke

NOTICES

Disclaimers

The findings in this report are not to be construed as an official Department of the Army position unless so designated by other authorized documents.

Citation of manufacturer's or trade names does not constitute an official endorsement or approval of the use thereof.

Destroy this report when it is no longer needed. Do not return it to the originator.

ARL-TR-9508 ● AUG 2022

Characterization of Fe_3O_4 Magnetosomes by Small-angle X-ray Scattering

Frederick L Beyer and Justin P Jahnke
DEVCOM Army Research Laboratory

Mark A Allen
General Technology Services

REPORT DOCUMENTATION PAGE	Form Approved OMB No. 0704-0188

1. REPORT DATE *(DD-MM-YYYY)*	2. REPORT TYPE	3. DATES COVERED (From - To)
August 2022	Technical Report	4 October 2021–2 May 2022

4. TITLE AND SUBTITLE	5a. CONTRACT NUMBER
Characterization of Fe_3O_4 Magnetosomes by Small-angle X-ray Scattering	5b. GRANT NUMBER
	5c. PROGRAM ELEMENT NUMBER

6. AUTHOR(S)	5d. PROJECT NUMBER
Frederick L Beyer, Mark A Allen, and Justin P Jahnke	5e. TASK NUMBER
	5f. WORK UNIT NUMBER

7. PERFORMING ORGANIZATION NAME(S) AND ADDRESS(ES)	8. PERFORMING ORGANIZATION REPORT NUMBER
DEVCOM Army Research Laboratory ATTN: FCDD-RLW-MG Aberdeen Proving Ground, MD 21005-5069	ARL-TR-9508

9. SPONSORING/MONITORING AGENCY NAME(S) AND ADDRESS(ES)	10. SPONSOR/MONITOR'S ACRONYM(S)
	11. SPONSOR/MONITOR'S REPORT NUMBER(S)

12. DISTRIBUTION/AVAILABILITY STATEMENT

Approved for public release: distribution unlimited.

13. SUPPLEMENTARY NOTES

ORCID ID: Frederick L Beyer, 0000-0003-0253-2134

14. ABSTRACT

Small-angle X-ray scattering was used to characterize magnetosome samples as found in *M. gryphiswaldense* bacteria, after extraction from the bacteria but dispersed in water, and in a powder form after drying. Samples of magnetosomes doped with cobalt were also characterized. The samples all scattered strongly and showed evidence of both form-factor and structure-factor scattering. In general, the magnetosomes formed chains of approximately 20 beads when contained in the bacteria. Once removed, the magnetosomes were only chaining in groups of two or three. When dried into a powder, a correlation peak starts to form in the low-q small-angle X-ray scattering data, suggesting aggregation. Finally, it was noted that the cobalt-doped magnetite particles tended to be slightly larger in diameter than those for the undoped magnetite.

15. SUBJECT TERMS

Biological and Biotechnology Sciences, Sciences of Extreme Materials, magnetosomes, SAXS, pearl necklace form factor

16. SECURITY CLASSIFICATION OF:			17. LIMITATION OF ABSTRACT	18. NUMBER OF PAGES	19a. NAME OF RESPONSIBLE PERSON
a. REPORT	b. ABSTRACT	c. THIS PAGE			Frederick L Beyer
Unclassified	Unclassified	Unclassified	UU	23	19b. TELEPHONE NUMBER (Include area code) (410) 306-0893

Contents

List of Figures

Acknowledgments

This work benefited from the use of the SasView application, originally developed under National Science Foundation award DMR-0520547. SasView contains code developed with funding from the European Union's Horizon 2020 research and innovation program under the SINE2020 project, grant agreement No. 654000. We would like to thank Superbrewed Food (SBF), Inc, Dr Biniam Maru, Dr Bryan Tracy, and Carrissa Wiedel for supplying magnetosomes and pasteurized magnetotactic bacteria created through chemostat fermentation (proprietary of SBF, Inc).

1. Introduction

Magnetosomes are naturally occurring vesicles comprising a phospholipid bilayer membrane and single crystal magnetite (Fe_3O_4) nanoparticle. They are produced naturally by magnetotactic bacteria such as *Magnetospirillum gryphiswaldense*.[1] Cells containing magnetosomes are sensitive to magnetic fields because the magnetosomes can form chain-like arrangements that allow the organisms to orient along magnetic field lines.[2] As the product of a biomineralization process, the magnetic nanoparticles themselves are generally well-defined in size and known to have a truncated tetrahedron shape.[1,3]

Magnetite nanoparticles are of interest because of their electronic and magnetic properties. Synthesis via magnetosomes offers a potentially low-cost route to manufacturing high-purity nanoparticles if efforts to grow magnetotactic bacteria and harvest magnetosomes are ultimately successful.[2] One possible application of synthetic magnetite nanoparticles could be in RF coatings, where the nanoparticles could affect properties including impedance. Doping the Fe_3O_4 magnetite structure with cobalt and other elements is also of interest for tuning the surface RF behavior of the magnetite particles.[4,5]

Characterizing the shape, average size, and size distribution of nanoparticles produced inside magnetosomes is important as it pertains to their physical properties. Magnetite particles synthesized inside magnetosomes are single-domain room-temperature ferromagnets.[6] At room temperature, particles smaller than 35 nm in diameter are superparamagnetic while larger magnetosomes are ferromagnetic, making characterization of size critically important.[7] Where direct characterization by transmission electron microscopy is time consuming and limited in the volume of material that can be observed in a single experiment, small-angle scattering (of X-rays or neutrons) is ideally suited for rapid, statistically robust measurement of nanoparticle size, shape, and spatial arrangement.[8–11] For particles having an average radius of gyration (R_g) between roughly 1 and 50 nm, laboratory-scale small-angle X-ray scattering (SAXS) is a convenient method for this analysis. In this report, the approach and results of magnetosome characterization will be describe for both Fe_3O_4 and cobalt-doped Fe_3O_4 magnetosomes.

2. Experimental

Four samples of magnetosomes containing Fe_3O_4 magnetite nanoparticles were provided by Superbrewed Food, Inc, which has developed reliably produced pure magnetosomes at low cost through a proprietary chemostat fermentation process.

Two samples were provided of magnetosomes from batch "3A," one at normal concentration and one diluted slightly with water during the sample preparation process. The remaining two samples comprised magnetosomes in which a small amount (3%–5%) of cobalt was substituted for the Fe^{3+} in the ferrite particles. One was at the starting concentration and one was diluted with water during the film preparation process. Powder samples were prepared by placing 20 μL of each magnetosome dispersion in water on a piece of Scotch-brand Magic tape and allowing it to dry in air at room temperature. To secure the dried material on the tape, a second piece of tape was applied to the dried droplet.

SAXS data were collected using a Xenocs "Xeuss 3.0 HR" SAXS instrument. X-rays were generated with a Rigaku MicroMax-007HF rotating copper (Cu) anode X-ray generator operated at 40 kV and 30 mA. The characteristic $Cu_{K\alpha}$ photons were monochromated and collimated using a focusing optic and two scatterless slit apertures, producing a well-aligned incident beam with wavelength (λ) of 1.5418 Å. Data were collected using a Dectris PilatusR 300k solid-state X-ray detector at three sample-to-detector distances (1800, 900, and 370 mm, respectively) to give a combined angular range of $0.003\ Å^{-1} < q < 0.7\ Å^{-1}$, where q is the modulus of the scattering vector, such that $q = 4\pi \sin(\theta)/\lambda$, where 2θ is the scattering angle. Isotropic two-dimensional data were azimuthally averaged to generate one-dimensional data, $I(q)$, for analysis. Silver behenate was used to calibrate the beam center and sample-to-detector distance.[12] In general, data processing and analysis were performed using Wavemetrics Igor Pro v8 and procedures available for download from Argonne National Laboratory.[13,14] SasView 5.0.4 was used for fitting the pearl necklace (PN) form factor specifically.

The raw scattering data were treated differently depending on the sample holder. For dry powder materials, samples were sandwiched between pieces of Scotch-brand Magic tape, the sample data were corrected for background scattering from the tape. While it was not possible to place the data on an absolute scale because the volume of material characterized was unknown, the data were still scaled using transmitted flux.[15] For liquid samples, a sample holder using quartz capillaries mounted in individual stainless-steel cassettes was used, allowing precise subtraction of the scattering background from each individual cassette.[16] The capillary diameters are nominally 2 mm, allowing these data to be placed on an approximate absolute scale.

X-ray scattering length densities were calculated for magnetite nanoparticles, a generic organic material to represent the phospholipid shell, and water. The values are $41.5 \times 10^{10}\ cm^{-2}$, $9.05 \times 10^{10}\ cm^{-2}$, and $9.3 \times 10^{10}\ cm^{-2}$, respectively.

3. Results and Discussion

The use of small-angle scattering for characterization of nanoparticles is well-established.[8,9,11] Depending on the instrument and size of the nanoparticles, SAXS can provide information on the particle shape, average size, size distribution, and aggregation. Scattering from such two-phase materials is the combination of form-factor scattering, $P(q)$, describing the particle shape, and structure-factor scattering, $S(q)$, describing the particles' spatial organization.[17] Equation 1 gives this relationship, where N is the number of scattering objects or domains:

$$I(q) = NP(q)S(q)\ , \tag{1}$$

where, $P(q)$ is the square of the scattering amplitude, $B(q)$, which itself is the Fourier transform of the scattering length density, ρ, throughout the particle. Equation 2 defines $B(q)$, where r is the correlation length in real space and ρ_0 is the average scattering length density throughout the sample[18]:

$$B(q) = 4\pi \int_0^\infty [\rho(r) - \rho_0]\, r^2\, \frac{\sin(qr)}{qr}\, dr\ . \tag{2}$$

Thus, the form factor has the form of an oscillating function that begins at relatively low q with a plateau that drops into a series of peaks ("fringes") with decreasing maximum intensity. The transition from the plateau to the first fringe is also known as the "Guinier knee," and can be approximated by the Guinier Law shown in Eq. 3. Here, R_g is the radius of gyration, the second moment of the electron density distribution. The Guinier approximation shows that as the size of the particle (R_g) increases, the position of the Guinier knee will shift to lower q. Likewise, a decrease in particle size will shift the Guinier knee to a higher range of q:

$$\lim_{q\to 0} I(q) \propto e^{-\frac{1}{3}q^2 {R_g}^2}\ . \tag{3}$$

In some cases exact solutions for the form factor are available. In the case of magnetite nanoparticles, which have the shape of a truncated tetrahedron, the form factor is nontrivial and not easily implemented.[19] However, in general, the form factor of a solid sphere can be used as an approximation and is easily implemented. The form factor for a solid sphere of uniform composition is given in Eq. 4[20]:

$$P(q,R) = \frac{4\pi}{3} R^3\, \frac{3[\sin(qR) - qR\cos(qR)]}{(qR)^3}\ , \tag{4}$$

where, the structure factor, $S(q)$, is the Fourier transform of the spatial organization of the individual domains and in general is difficult to calculate. For an organized

material, such as a block copolymer ordered into a lattice, the structure factor is the familiar Bravais lattice in reciprocal space (body-centered cubic, Q^{230} gyroid, etc.). For less organized materials, *S(q)* is described by Eq. 5, where *g(r)* is the radial distribution function describing the relative locations of the scattering objects in space[21]:

$$S(q) = 1 + 4\pi \int_0^r [g(r) - 1] r^2 \frac{\sin(qr)}{qr} dr \ . \quad (5)$$

In a recent publication,[22] the pearl necklace form factor[23] was applied to scattering from magnetosomes to account for the tendency of magnetite nanoparticles to form chains of particles in magnetotactic bacteria. The PN form factor uses the result for a solid sphere from Eq. 4 and cannot be applied in conjunction with a core-shell primary particle geometry.

Figure 1 shows the SAXS data collected for the lipid-functionalized magnetosomes in three environments, as well as that collected for the cobalt-doped magnetite particles. In all cases, form-factor scattering is observed, with a Guinier knee around q = 0.02 Å^{-1}, and up to three form-factor fringes at higher angles. At angles lower than 0.02 Å^{-1}, instead of the smooth turn to a plateau expected for dilute nanoparticles, two different behaviors are observed. For the magnetosomes in solution (blue), magnetosomes (3A) in solution (green), and cobalt-doped magnetosomes in solution (black), the low-q data have a distinctive shape characterized by a noticeable change in slope around 0.015 Å^{-1}. The data from magnetosomes in bacteria (red), magnetosomes in dry powder form after extraction from bacteria (yellow), and the cobalt-doped magnetosomes as a dry powder after extraction (orange) also exhibit characteristic low-q scattering, with a weak correlation peak around 0.015 Å^{-1}. Each data set will be analyzed and discussed in turn.

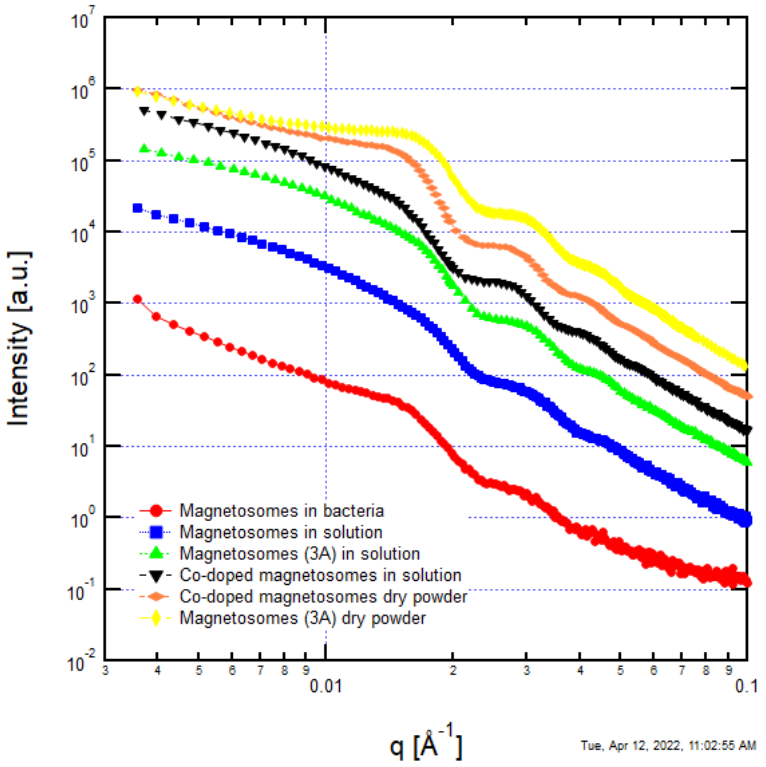

Fig. 1 SAXS data collected for the two magnetosome samples

Figure 2 provides the results of model fitting for both a core-shell sphere particle form factor (blue) and a PN cylinder form factor (red) to the data for *M. gryphiswaldense* bacteria in water. The data were corrected for scattering from the glass capillary sample holder, but the scattering from water was explicitly included in the core-shell form factor as the solvent phase. The core-shell model best fits the data for a magnetite core 39.0 nm in diameter, a Gaussian distribution of 3.3-nm core radii, and a shell of organic material 4.7-nm-thick. The PN model fits the data well at low-q, where it suggests that chaining is occurring with 20 nanoparticles in a chain,* but poorly above the Guinier region. The fitting parameters for the PN model were spheres having a diameter of 35 nm, and a sphere-to-sphere edge separation of 7.1 nm. It is clear that neither the core-shell form factor nor the PN form factor fully account for the observed scattering. In the case of the core-shell model, no interactions between the nanoparticles are included. The PN model does not account for the core-shell nature of the magnetite particles or for the specific shape of the particles. This may explain why the particle size returned from the PN model is smaller than that from the core-shell sphere model.

* The fitting procedure in SasView for the PN form factor did not vary the parameter for number of beads in the PN chain, requiring the user to manually fit the parameter.

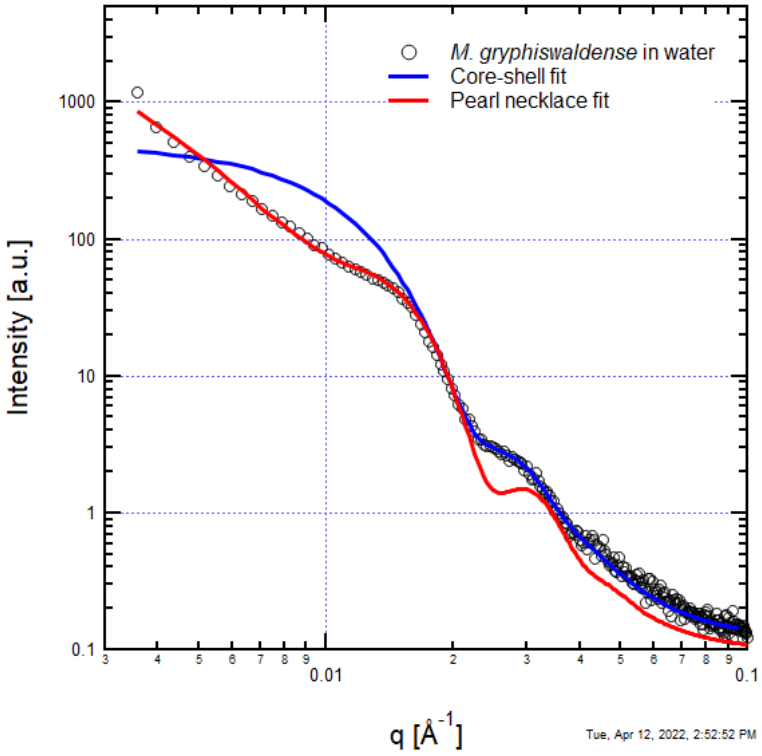

Fig. 2 SAXS data (black) and results of model fitting for *M. gryphiswaldense* in solution

Figure 3 shows the results of fitting the core-shell sphere form factor and the PN form factor to the SAXS data for magnetosomes extracted from *M. gryphiswaldense* bacteria. The magnetosomes here are suspended in water. The scattering from this sample was stronger and a second form-factor fringe is visible in the data around 0.045 $Å^{-1}$. Although the core-shell sphere form factor fits the first fringe (0.03 $Å^{-1}$), it fails to fit this second fringe, an indication that the core-shell sphere model is not correct. Li et al. demonstrated how platonic solids with higher numbers of sides have a shift in the form-factor fringe positions from those for a solid sphere.[19] In the fitting process here, the best fit was obtained when the first form-factor fringe was fit well, to the detriment of higher order fringes, through an increase in the particle size dispersity (width of Gaussian distribution). A narrower distribution of particle diameters was required to reveal the second order form-factor fringe, resulting in a lower quality fit. This effect is therefore attributed to the use of a model for spheres rather than a model specifically for truncated tetrahedra.

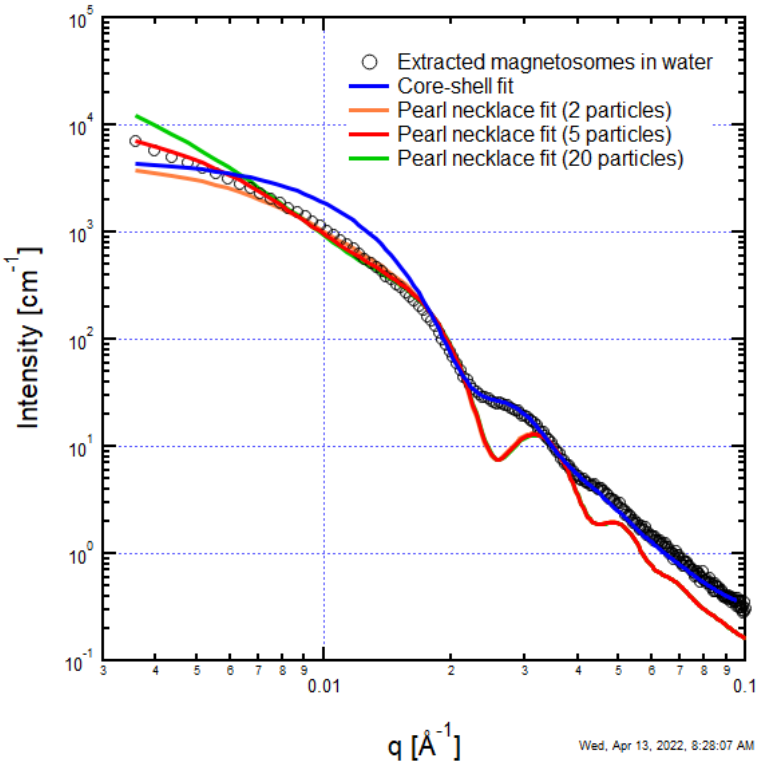

Fig. 3 SAXS data (black) for extracted magnetosomes in water, and the resulting model fits for a core-shell sphere (blue), and PNs with 5 beads (red), 2 beads (orange), and 20 beads (green)

Figure 3 also shows three different fits for the PN model. The fit for five beads (nanoparticles) fits the general shape of the low-*q* scatter very well. Here, the particle diameter is again 35 nm, but in this case the particle edge-to-edge separation for the fit is 0 nm.* As with the magnetosomes in bacteria (Fig. 2), these differences are likely due to the hard-sphere basis of the PN form factor. To illustrate the effect of chaining on the scattering data, model fits for 2 and 20 beads are also included in Fig. 3. The effect is most pronounced at the lowest angles, where the larger chain lengths push the model intensity up, but it is also visible around 0.008 Å^{-1}, where an inflection point develops in the form factor, leading to the development of a weak correlation peak at 0.018 Å^{-1}.

Figure 4 shows the scattering data from magnetosomes from batch "3A" (black) and the results of modeling using the core-shell form-factor approach used in Fig. 3 (blue). When fit alone, the core-shell model again fails to capture the detail of the scattering data beyond the first form-factor fringe (0.03 Å^{-1}). The fit indicates that the magnetite nanoparticle core is 38.7 nm in diameter, with an organic shell

* A value of zero for the edge-to-edge separation causes the model to fail. A value of 0.01 nm was used instead.

3.2-nm-thick. The results of the PN form-factor fit are excellent in this case and indicate that the magnetite particles are 36 nm in diameter, with an average of two beads per chain.

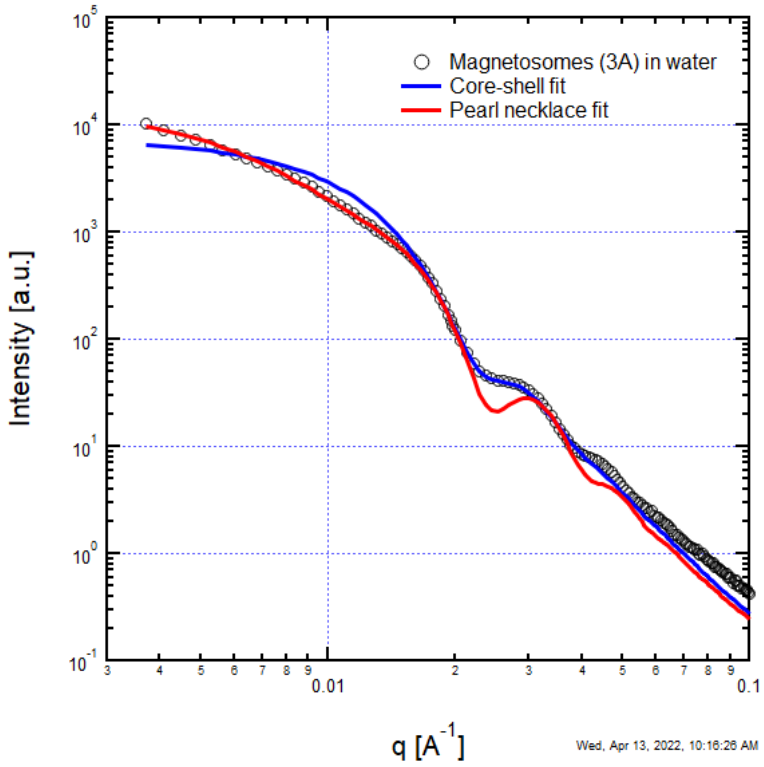

Fig. 4 SAXS data (black) for magnetosomes from batch "3A" in water, and model fit results for a core-shell sphere (blue) and a PN (red)

Figure 5 shows the scattering data from the magnetosomes from batch 3A characterized after a droplet of a concentrated aqueous dispersion was allowed to dry on a piece of tape. The fitting procedure for the core-shell model was applied, resulting in a magnetite core diameter of 38.8 nm and an organic shell thickness of 1.0 nm. The PN form factor was unable to capture the shape of the low-q scattering, which now includes a correlation peak at roughly 0.017 Å^{-1}. This suggests that the nanoparticles are no longer forming chains and are instead aggregating.

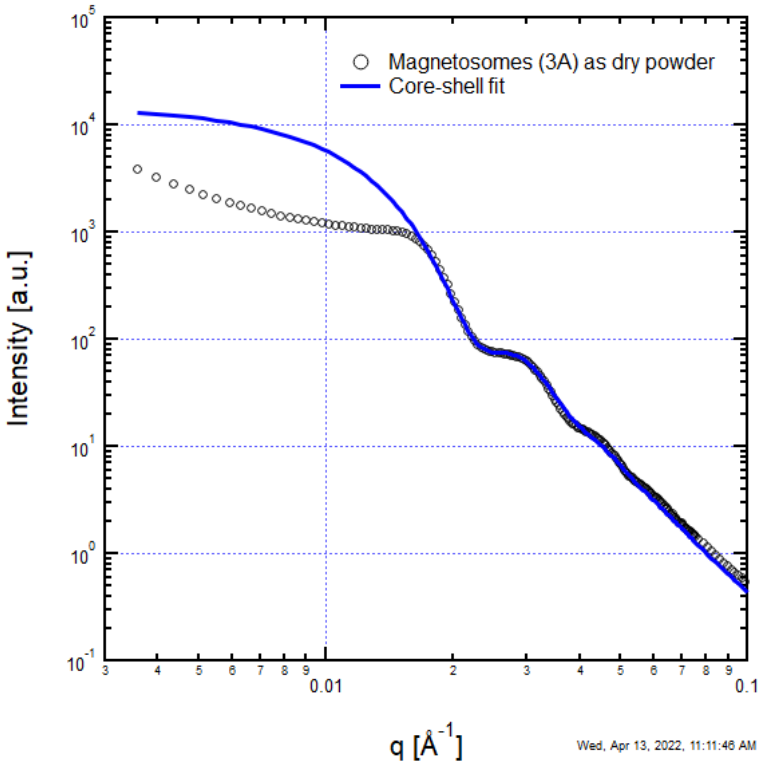

Fig. 5 SAXS data for dry powder magnetosomes (black) and the resulting fit of the core-shell model (blue)

Comparison of the data from Fig. 5 and that of a more dilute sample of the sample magnetosomes as shown in Fig. 6 reveal that there is background scattering present even after the data were corrected using the normal procedures—as indicated by the convergence of both data sets at high-q and low-q. To account for this background, an empirically determined power law of $q^{-3.0}$ was added to the scattering from a sphere form factor and a hard-sphere structure factor. The resulting fit is much better than the PN or core-shell form factor fits individually, but still returns questionable values for separation between magnetite cores. The sphere form factor indicates that the cores are 39.7 nm in diameter, ±4.8 nm, but the hard-sphere structure factor fits the data best when the center-to-center distance between sphere is only 30.6 nm. This nonphysical result suggests that there may be additional structure in the material for which these specific models are unable to account.

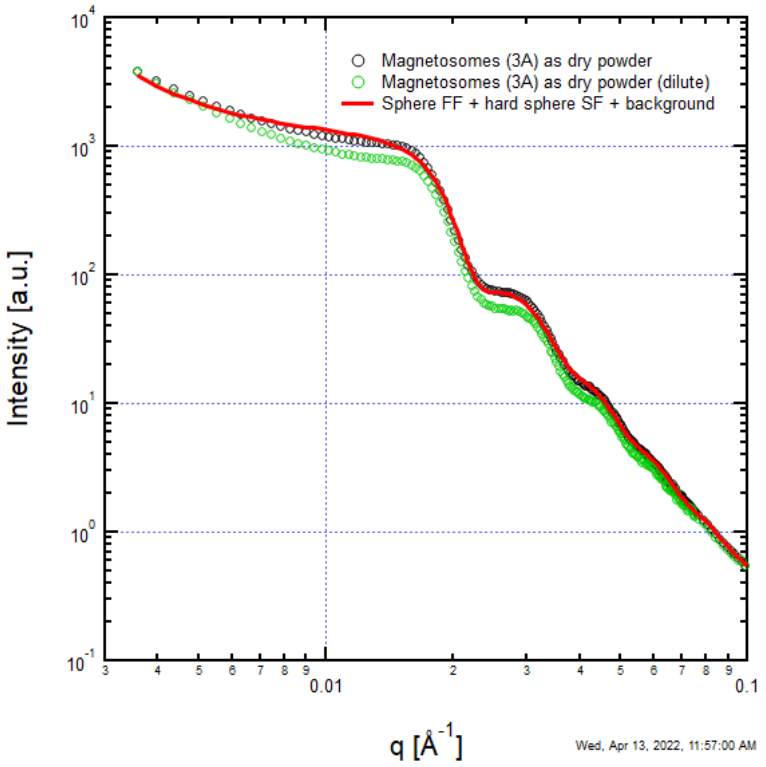

Fig. 6 SAXS data for dry magnetosomes (black) and dilute dry magnetosomes (green), and the results of model fitting (red)

Finally, a set of magnetosomes grown in a cobalt-rich environment were also characterized in this study. The SAXS data for these magnetosomes, shown in Fig. 1 as a dispersion in water (orange) and as a dry powder (black), are nearly identical to the data collected for the undoped magnetosomes from batch 3A. Analyzing the data in the same fashion reveals that the cobalt-doped nanoparticles are generally larger than their undoped counterparts. Figure 7 shows the results of the core-shell form factor fit (blue) and the PN form factor fit (red). The core-shell model returns a magnetite core diameter of 42.2 nm (±6.2 nm) with an organic shell 5.7-nm-thick. The PN model suggests that the magnetosomes are chaining in groups of three but returns a bead diameter of only 38.8 nm. In Fig. 8, the data from both the concentrated and diluted cobalt-doped magnetosome suspensions after drying on tape are shown. The data for the concentrated powder were fit using the same approach as for the undoped magnetosomes (Fig. 6), with a hard-sphere form factor, hard-sphere structure factor, and a power law background proportional to $q^{-3.15}$. This model indicates that the cobalt-doped nanoparticles have a diameter of 42.8 nm (±4.0 nm). However, the hard-sphere structure factor returns a particle spacing of 32.2 nm, which is a similar nonphysical result as that obtained for the undoped magnetosome. This suggests that these models are not accurately capturing the spatial organization of the magnetosomes, which is clearly not dilute.

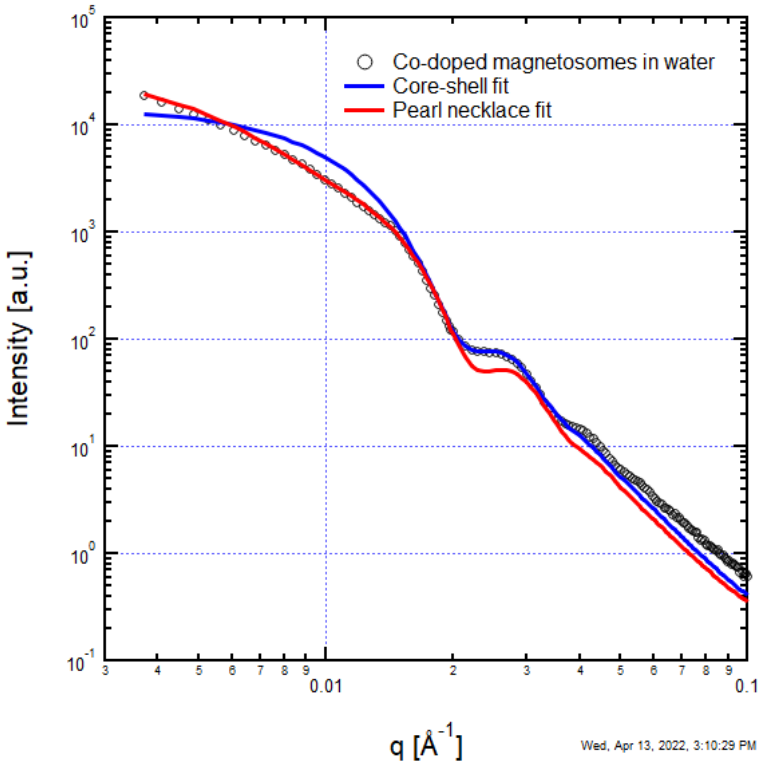

Fig. 7 SAXS data for cobalt-doped magnetosomes in water (black), the core-shell model fit results (blue), and the PN model fit results (red)

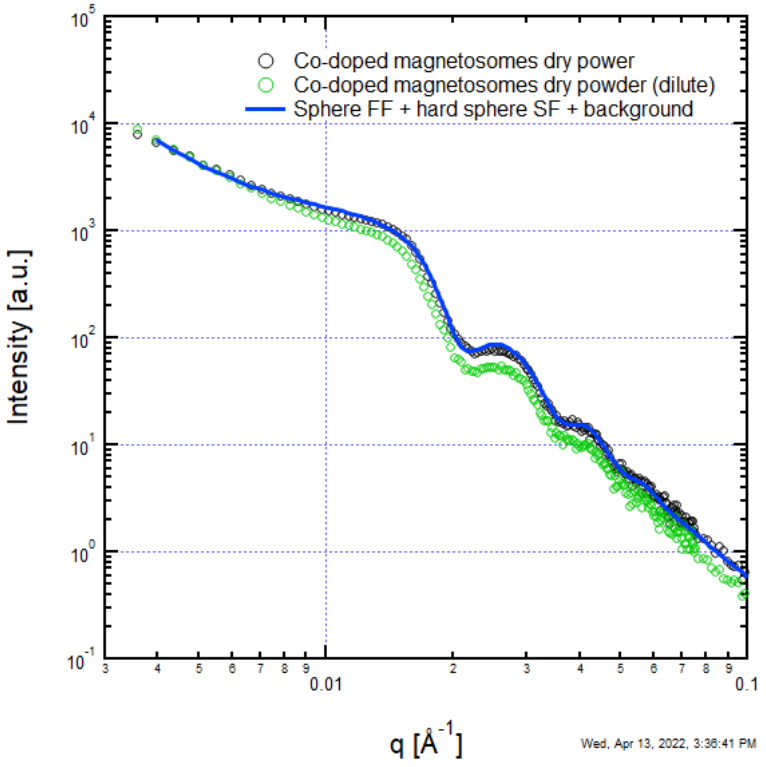

Fig. 8 SAXS data for cobalt-doped magnetosomes as dry powder and resulting model fit

4. Summary and Conclusion

SAXS was used to characterize magnetosome samples as found in *M. gryphiswaldense* bacteria, after extraction from the bacteria but dispersed in water, and in a powder form after drying. Samples of magnetosomes doped with cobalt were also characterized. The samples all scattered strongly and showed evidence of both form-factor and structure-factor scattering. The form factor for a core-shell sphere was used to fit the form-factor fringes but was found to fit higher order form factor maxima poorly. This effect was attributed to the difference between scattering from platonic solids with a low number of sides, such as the truncated tetrahedra of magnetite. For the data collected from bacteria and after extraction, the low-angle data could be fit with the PN form factor, which models scattering centers as beads on a string. In general, the magnetosomes formed chains of approximately 20 beads when contained in the *M. gryphiswaldense* bacteria. Once removed, the PN model suggested that the magnetosomes were only chaining in groups of two or three. This effect can be seen upon visual inspection of the low-q SAXS data. Once dried into a powder, a correlation peak starts to form in the low-q SAXS data, suggesting aggregation. The PN form factor is not able to fit these data, but the Percus–Yevick hard-sphere structure factor, for spheres on a liquid-like lattice, does capture the general trends. In these dry-powder samples, the form factor for a sphere fits the observed form-factor scattering. However, the diameter of the sphere calculated using the form factor is larger than the calculated spacing between domains from the structure factor—a nonphysical result indicating spatial organization other than spheres on a liquid-like lattice. Finally, it was noted that the cobalt-doped magnetite nanoparticles tended to be slightly larger in diameter than comprising undoped magnetite.

5. References

1. Lefevre CT, Bazylinski DA. Ecology, diversity, and evolution of magnetotactic bacteria. Microbiol Mol Biol Rev. 2013;77:497–526.

2. Komeili A. Molecular mechanisms of compartmentalization and biomineralization in magnetotactic bacteria. Fems Microbiol Rev. 2012;36:232–255.

3. Orue I, Marcano L, Bender P, Garcia-Prieto A, Valencia S, Mawass MA, Gil-Carton D, Alba Venero D, Honecker D, Garcia-Arribas A, Fernandez Barquin L, Muela A, Fdez-Gubieda ML. Configuration of the magnetosome chain: a natural magnetic nanoarchitecture. Nanoscale. 2018;10:7407–7419.

4. Larumbe S, Gomez-Polo C, Perez-Landazabal JI, Garcia-Prieto A, Alonso J, Fdez-Gubieda ML, Cordero D, Gomez J. Ni doped Fe_3O_4 magnetic nanoparticles. J Nanosci Nanotechnol. 2012;12:2652–2660.

5. Marcano L, Munoz D, Martin-Rodriguez R, Orue I, Alonso J, Garcia-Prieto A, Serrano A, Valencia S, Abrudan R, Fernandez Barquin L, Garcia-Arribas A, Muela A, Fdez-Gubieda ML. Magnetic study of co-doped magnetosome chains. J Phys Chem C. 2018;122:7541–7550.

6. Yan L, Zhang S, Chen P, Liu H, Yin H, Li H. Magnetotactic bacteria, magnetosomes and their application. Microbiological Research. 2012;167:507–519.

7. Alphandery E, Ngo AT, Lefevre C, Lisiecki I, Wu LF, Pileni MP. Difference between the magnetic properties of the magnetotactic bacteria and those of the extracted magnetosomes: influence of the distance between the chains of magnetosomes. J Phys Chem C. 2008;112:12304–12309.

8. Li T, Senesi AJ, Lee B. Small angle X-ray scattering for nanoparticle research. Chem Rev. 2016;116:11128–11180.

9. Schaefer DW, Justice RS. How nano are nanocomposites? Macromolecules. 2007;40:8501–8517.

10. Rosenfeldt S, Riese CN, Mickoleit F, Schuler D, Schenk AS. Probing the nanostructure and arrangement of bacterial magnetosomes by small-angle X-ray scattering. Appl Environ Microbiol. 2019;85:e01513–01519.

11. Krueger S, Olson GJ, Rhyne JJ, Blakemore RP, Gorby YA, Blakemore N. Small-angle neutron and X-ray-scattering from magnetite crystals in magnetotactic bacteria. J Magn Magn Mater. 1989;82:17–28.

12. Huang TC, Toraya H, Blanton TN, Wu Y. X-ray-powder diffraction analysis of silver behenate, a possible low-angle diffraction standard. J Appl Crystallogr. 1993;26:180–184.

13. Ilavsky J, Jemian PR. Irena: tool suite for modeling and analysis of small-angle scattering. J Appl Crystallogr. 2009;42:347–353.

14. Ilavsky J. Nika: software for two-dimensional data reduction. J Appl Crystallogr. 2012;45:324–328.

15. Pauw BR. Everything SAXS: small-angle scattering pattern collection and correction. J Phys: Condens Matter. 2013;25:383201.

16. Knaapila M, Svensson C, Barauskas J, Zackrisson M, Nielsen SS, Toft KN, Vestergaard B, Arleth L, Olsson U, Pedersen JS, Cerenius Y. A new small-angle X-ray scattering set-up on the crystallography beamline I711 at MAX-lab. J Synchrot Radiat. 2009;16:498–504.

17. Roe R-J. Methods of X-ray and neutron scattering in polymer science. Oxford University Press, 2000.

18. Seelenmeyer S, Deike I, Rosenfeldt S, Norhausen C, Dingenouts N, Ballauff M. Small-angle X-ray and neutron scattering studies of the volume phase transition in thermosensitive core-shell colloids. J Chem Phys. 2001;114:10471–10478.

19. Chen W-R, Herwig KW, Li X, Liu E, Pynn R, Shew C-Y, Smith GS, Myles DAA, He L, Meilleur F. Scattering functions of platonic solids. J Appl Crystallogr. 2011;44:545–557.

20. Pedersen JS. Analysis of small-angle scattering data from colloids and polymer solutions: modeling and least-squares fitting. Adv Colloid Interface Sci. 1997;70:171–210.

21. Wood EL. Personal communication. University of Sheffield, 2019.

22. Rosenfeldt S, Riese CN, Mickoleit F, Schuler D, Schenk AS. Probing the nanostructure and arrangement of bacterial magnetosomes by small-angle X-ray scattering. App Environ Microbiol. 2019;85:12.

23. Schweins R, Huber K. Particle scattering factor of pearl necklace chains. Macromol Symp. 2004;211:25–42.

List of Symbols, Abbreviations, and Acronyms

Cu	copper
Fe_3O_4	single crystal magnetite
PN	pearl necklace
R_g	radius of gyration
RF	radio frequency
SAXS	small-angle X-ray scattering
SBF	Superbrewed Food, Inc

1 (PDF)	DEFENSE TECHNICAL INFORMATION CTR DTIC OCA
1 (PDF)	DEVCOM ARL FCDD RLD DCI TECH LIB
3 (PDF)	DEVCOM ARL FCDD RLH BA M ALLEN J JAHNKE FCDD RLW MG F BEYER